# HREELS and XPS Studies of Ferrocene on Ag(100)†

**C. M. Woodbridge,‡ D. L. Pugmire,‡ R. C. Johnson,‡ N. M. Boag,§ and M. A. Langell*,‡**

*Department of Chemistry and Center for Materials Research and Analysis, University of Nebraska, Lincoln, Lincoln, Nebraska 68588-0304, and Department of Chemistry, University of Salford, Salford, M5 4WT U.K.*

*Received: September 13, 1999; In Final Form: November 17, 1999*

High-resolution electron energy loss spectroscopy (HREELS) and X-ray photoelectron spectroscopy (XPS) have been used to investigate the adsorption of ferrocene on Ag(100) at 150 K. The HREELS data show that ferrocene adopts an orientation with the molecular axis perpendicular to the Ag(100) surface plane for low exposures. Additionally, no rehybridization is observed at the low temperature employed. Upon multilayer growth, however, the molecular axis becomes canted with respect to the surface normal. XPS for monolayer ferrocene gives Fe 2p binding energies of 707.9 and 720.8 eV for the $2p_{3/2}$ and $2p_{1/2}$ transitions, respectively, and C 1s binding energy of 284.9 eV. Monolayer surface coverage represents a molecular footprint of about one ferrocene per nine Ag surface atoms. Multilayer ferrocene grows in a layer-by-layer fashion and shows HREELS and XPS

## I. Introduction

Metallocenes are organometallic compounds in which a metal cation is ligated to cyclic aromatics through their delocalized $\pi$ orbitals. Perhaps the best known, and first reported,[1] metallocene is ferrocene, $Fe(C_5H_5)_2$, which is a "sandwich" compound where the two cylopentadienyl (Cp or $C_5H_5^-$) rings sit above and below the $Fe^{2+}$ ion. Metallocenes, of which ferrocene can be considered prototypical, have found applications[2,3] in a number of diverse areas including fuel additives to improve combustion and eliminate smoke, antiknock agents, components in coatings for missiles and/or satellites, high-temperature lubricants, dopants to stabilize organics and polymers against UV degradation, photopolymerization catalysts, combustion catalysts for solid propellants, tethered biosensors for redox enzymes,[4] barium and calcium ion-sensitive electrodes,[5] and surfactants.[6]

Many organometallic compounds, including ferrocene, decompose readily[7] under electron or photon irradiation and therefore can be used as selectively activated chemical vapor deposition (CVD) source molecules for the formation of thin metal films on a variety of substrates. When CVD conditions and source molecules are chosen appropriately, CVD can be a clean, controllable means of depositing these films. The CVD[7,8] properties of metal carbonyls such as $Fe(CO)_5$ have been extensively investigated. While $Fe(CO)_5$ is a highly toxic[9] liquid, ferrocene is a less toxic solid. Therefore, ferrocene and other metallocenes may be better choices for CVD molecules because of their more suitable handling properties. Additionally, the metallocenes may deposit more cleanly and with greater spatial control.

Ferrocene has an extraordinary thermal stability to temperatures greater than 773 K but yet possesses sufficiently high vapor pressure[10] (0.966 Pa at 298 K) to make it a reasonable candidate for CVD transport[11,12] of the metal to a substrate. Once physisorbed upon the substrate, irradiation of the metallocene with either a photon or an electron beam will cause the ligands to desorb, which leaves the metal behind "written" onto the substrate in features with resolution limited primarily by that of the beam used to stimulate decomposition of the precursor molecule. In the absence of irradiation, ferrocene desorbs[11,12] from Ag(100) intact at 250 K and at approximately this value for other substrates[11,12] on which it physisorbs. Prototype nanoscale wires and semiconductor devices have been reported with features as small as 5 nm in width[13−15] for photo- and electron-assisted CVD of ferrocene and related metallocene molecules.

Despite the promise that metallocenes hold for use as CVD source molecules, very few studies have been performed to elucidate either the nature of their bonding to solid substrates or their electron, photon, and thermal decomposition pathways mediated by solid substrates. Ferrocene adsorption on Ag(100) has been studied by angle-resolved photoemission (ARPES)[12,16] and the data obtained are consistent with molecular adsorption with the molecular axis oriented perpendicular or nearly perpendicular to the substrate surface plane. Because of ARPES detection limitations, the study was limited to ferrocene films several monolayers thick. Monolayer or near-monolayer exposures of ferrocene have also been investigated by scanning tunneling microscopy/high-resolution electron energy loss spectroscopy (STM/HREELS)[12,16] and angle-resolved thermal desorption[11,12] on Ag(100) and by STM/HREELS on graphite[17] to confirm that ferrocene adsorbs in an upright orientation on these substrates.

We report here $FeCp_2$/Ag(100) X-ray photoelectron (XPS) and HREELS spectra as a function of adsorbate coverage for submonolayer to multilayer concentrations. XPS is used to provide quantitative measurement of the metallocene adsorbate concentration as well as information on the iron and cyclopentadienyl oxidation states. The HREEL spectra are compared to literature IR data[18,19] and normal coordinate analysis[19,20] of the isolated ferrocene molecule. The HREELS data presented in this paper agree with previous observations of the molecular orientation but are more extensive in scope than have been previously reported. Additionally, the resolution is substantially

† Part of the special issue "Gabor Somorjai Festschrift".

* To whom correspondence should be addressed. Phone: (402) 472-2702. Fax: (402) 472-9402. E-mail: mlangell@unlserve.unl.edu.

† University of Nebraska.

‡ University of Salford.

10.1021/jp993235+ CCC: $19.00 
Published on Web 01/07/2000

improved over previously reported spectra to allow for unprecedented detail in the analysis of the adsorbate vibrational modes. Information on adsorbate−substrate bond strength and other features of $FeCp_2$/Ag(100) bonding will be described in detail below.

## II. Experimental Methods

The experimental ultrahigh vacuum chamber is operated at a base pressure of $5 \times 10^{-10}$ Torr and has been described previously.[21] The HREEL spectrometer (LK2000) is equipped with a double 127° sector analyzer for monochromatizing the incident beam and a third sector for electron energy analysis. The spectrometer is routinely operated with resolution of about 5−7 meV (40−56 $cm^{-1}$), as measured by the full width at half-maximum (fwhm) of the elastically scattered beam, and a sample current of 70−90 pA. Electrons are incident to the surface at 60° measured relative to the surface normal. The primary energy of the incident electron beam was 3.77 eV unless otherwise noted.

XP spectra were acquired in the pulse-count, constant pass energy mode using a Physical Electronics 15-255G cylindrical mirror analyzer. Data were obtained using a pass energy of either 200 or 50 eV as noted in the figure captions. XP spectra were generated with Mg Kα (1253.6 eV) radiation and were signal-averaged with dwell times of 50 ms and pulse-count step sizes of 0.1 eV. The reported binding energies are calibrated by setting the Ag $3d_{5/2}$ substrate peak to 367.9 eV.[22] Errors in reported peak positions are ±0.2 eV.[23]

An Ag(100) single crystal (Goodfellow, oriented to ±0.5° of the (100) plane) was mounted on the end of the sample manipulator that is capable of both resistive heating and cooling to liquid nitrogen temperatures. The sample temperature was monitored with a chromel−alumel K-type thermocouple held in thermal contact with the crystal. Sample cleaning was performed using repeated cycles of $Ar^+$ bombardment at 0.5 kV for 20 min at 623 K with a sample current of approximately 5 $\mu A/cm^2$ at the surface and annealing at 673 K for 30 min until the surface was determined to be clean by Auger electron spectroscopy (AES).

The clean Ag(100) surface was dosed with either ferrocene or deuterated ferrocene, $Fe(C_5D_5)_2$, via admission of the gas through a standard leak valve that has been equipped with a needle doser that concentrates the metallocene vapor in the vicinity of the sample surface. While no impurities were detected for $Fe(C_5H_5)_2$ by mass spectrometric techniques, the deuterated ferrocene was contaminated with about 15% protonated $Fe(C_5H_5)_2$ and $Fe(C_5H_5)(C_5D_5)$ materials. Exposures with the present experimental dosing configuration were calibrated to dosage time by comparison with previously reported[12] data, which indicate that ferrocene saturates at monolayer coverage after a 10 langmuir exposure.

No decomposition of the adsorbed metallocene into metallic iron and cyclopentadiene was observed during the acquisition of either XP or HREEL spectra. No features due to metallic iron are present in the AES spectrum after allowing the substrate to warm to room temperature. The primary beam energy used in the acquisition of HREEL spectra is below the ionization potential of gaseous ferrocene[12] and below the metal−ligand bond dissociation energy.[12] Therefore, no electron-induced decomposition is expected. The incident photon energy used to acquire XP spectra is well above the ionization potential, and to ensure no decomposition had occurred during XPS acquisition, HREEL spectra were obtained both prior to and following irradiation of the ferrocene-covered adsorbate by Mg Kα photons. The lack of detectable decomposition is most likely due to a combination of low X-ray fluence and low cross section for excitation of valence electrons[24] at XPS energies.

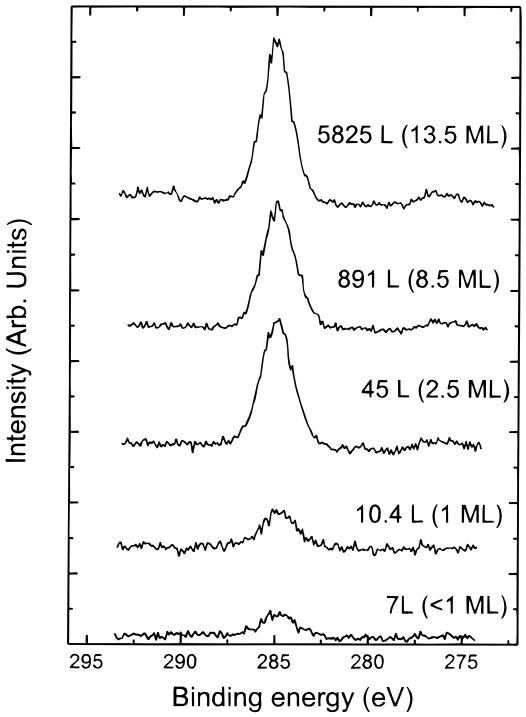


**Figure 1.** C 1s XP spectra as a function of exposure. Exposures are indicated in the figure, and data were acquired at a pass energy of 50 eV.

## III. Results

**A. XPS Data.** XP spectra of the carbon 1s and iron 2p regions were acquired in order to provide information about the chemical environment of the carbon and iron in ferrocene. The data are presented in Figures 1 and 2, respectively. For very long exposures, the C 1s XP spectrum is composed of a single peak with a binding energy of 285.0 eV and a fwhm of 2.9 eV. This binding energy is characteristic of carbon in a Cp ($Cp = C_5H_5^-$) ring that has ligated to the iron cation in bulklike ferrocene films. Low exposures also result in a single C 1s peak with a binding energy of 284.9 eV, and the fwhm is 2.3 eV. Carbon 1s binding energies for monolayer and multilayer ferrocene are indistinguishable within the error of the measurement. It was not possible to resolve more than one core state level for the C 1s XP spectrum of the monolayer ferrocene, and therefore, the two Cp rings are indistinguishable within the resolution of the present XPS analysis.

Unfortunately, interference from Ag 3s photoemission coupled with the low concentration of the iron in the ferrocene molecule limits the usefulness of the Fe 2p data at low exposures. At or below monolayer coverages, the Fe 2p region is dominated by the Ag 3s peak. However, this region can be curve-resolved in order to estimate the binding energy of the $2p_{3/2}$ peak to be 707.9 eV. As exposure is increased, the binding energy of the Fe $2p_{3/2}$ peak is observed at 708.1 eV for bulklike films. The Fe $2p_{3/2}$ binding energies observed in the present work for monolayer and multilayer coverage are in good agreement with literature values[25,26] but are lower than what one would expect for iron in an ionic +2 oxidation state. A Mulliken population analysis[27] of ferrocene indicates that the iron atom bears a charge of approximately +0.6 to +0.8, which is reasonably consistent with the binding energies observed in this study. A summary

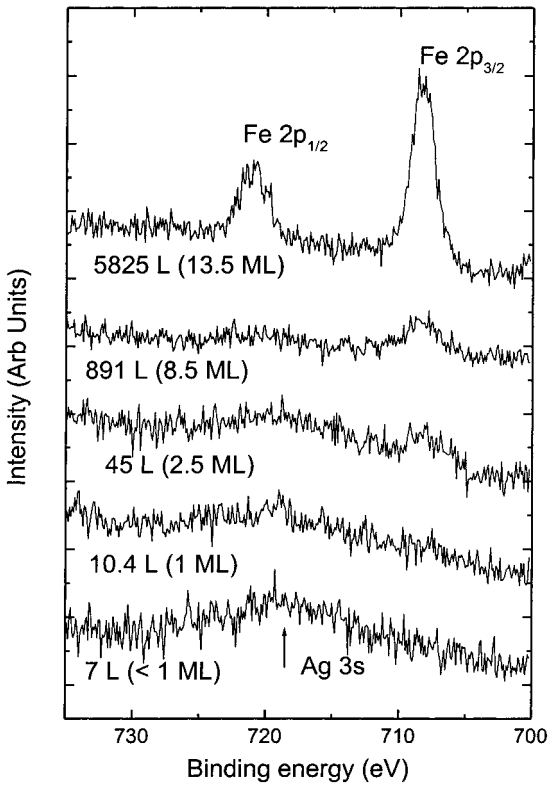


**Figure 2.** Fe 2p XP spectra as a function of exposure. Exposures are indicated in the figure, and data were acquired at a pass energy of 50 eV.

**TABLE 1: Binding Energies Observed for Ferrocene and Deuterated Ferrocene with Uncertainties in Peak Positions of ±0.2 eV**

| | C 1s (eV) | Fe $2p_{3/2}$ (eV) | Fe $2p_{1/2}$ (eV) |
|---|---|---|---|
| monolayer | | | |
| $Fe(C_5H_5)_2$ | 284.9 | 707.9[a] | 720.8[a] |
| $Fe(C_5D_5)_2$ | 284.8 | 707.7[a] | 720.5[a] |
| multilayer | | | |
| $Fe(C_5H_5)_2$ this work | 285.0 | 708.1 | 721.0 |
| ref 25 | 284.7 | 707.9 | not reported |
| ref 26 | | 708.0 | 720.7 |
| $Fe(C_5D_5)_2$, this work | 284.8 | 707.8 | 720.6 |

[a] Estimated by curve resolving peak from Ag 3s.

of C 1s and Fe 2p binding energies is given in Table 1, along with comparable data for the deuterated ferrocene analogue.

Information on the ferrocene surface concentration is provided in Figure 3 where the C 1s/Ag 3d XPS intensity ratio is plotted as a function of exposure. Although concentration information can be determined more rapidly using AES, the Auger beam readily decomposes ferrocene to leave metallic iron on the surface. Therefore, AES is not a viable method for surface coverage analysis in this case. The silver surface was exposed to a series of doses of ferrocene or deuterated ferrocene, and XP spectra were acquired for the C 1s and Ag 3d regions after each dose. Intensities were determined from the XP peak areas for each spectral region, and the intensity ratios, $I_C/I_{Ag}$, are plotted in Figure 3. The carbon uptake rate shows a change in slope at $I_C/I_{Ag} = 0.023 \pm 0.008$ attributed to completion of the first monolayer of ferrocene. Deuterated ferrocene shows a similar uptake curve with monolayer completion at $I_C/I_{Ag} = 0.028 \pm 0.006$ equivalent to that of the ferrocene to within the error of the measurement.

Peak intensity information can be used to obtain the relative atomic concentrations using photoemission cross sections[28] and

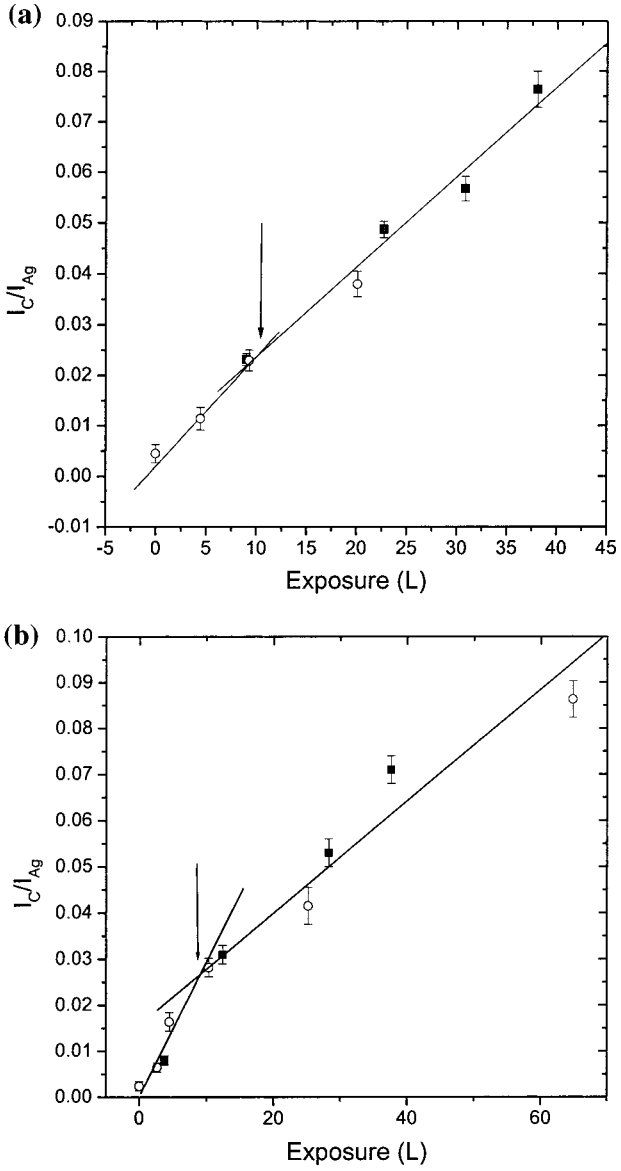


**Figure 3.** Uptake curve of $Fe(C_5H_5)_2$ (a) and $Fe(C_5D_5)_2$ (b) obtained from C 1s and Ag 3d XP spectra. The arrow indicates the point where the change in slope for carbon uptake occurs. Data were acquired at a pass energy of 200 eV. Symbols indicate two different trials. The error due to uncertainties in the measurement and integrating procedure is determined to be less than 15%.

assuming an exponential attenuation of electrons with depth:[29]

$$\frac{I_C}{I_{Ag}} = \frac{C_C\sigma_C}{C_{Ag}\sigma_{Ag}I^{\infty}_{Ag}\exp\left(-\frac{y}{\lambda_2\cos\theta}\right)} \quad (1)$$

where

$$I^{\infty}_{Ag}\sum_{n=0}^{\infty}\exp\left(\frac{-nx}{\lambda_1\cos\theta}\right) \quad (2)$$

In the above equations, the subscript $i$ depicts the element of interest, either carbon or silver. $I_i$ is the area of the XPS peak from the $i$th element, $\sigma_i$ is its photoionization cross section, $C_i$ the concentration, $y$ the distance from Cp ligand to Cp ligand for ferrocene inclusive of van der Waal radii, $x$ the lattice spacing of Ag(100), $\theta$ the photoemission detection angle, and $\lambda_i$ the mean free path of an 885 eV Ag $3d_{5/2}$ electron passing

**TABLE 2: Parameters Used To Evaluate $C_C/C_{Ag}$ for One Monolayer of Ferrocene[a]**

| parameter | value |
|---|---|
| $\sigma_C$ (a) | 1.00 (×22000 barns) |
| $\sigma_{Ag}$ (a) | 18.04 (×22000 barns) |
| $\lambda_1$ (b) | 11.8 Å |
| $x_{Ag}$ (c) | 2.89 Å |
| $\lambda_2$ lower estimate (b) | 11.8 Å |
| $\lambda_2$ higher estimate | ∞ |
| $x_{FeCp2}$ (d) | 7.00 Å |
| $\theta$ (e) | 41° |

[a] Letters in parentheses indicate the following references: (a) ref 28, (b) ref 30, (c) ref 16, (d) refs 31−32, and (e) ref 33.

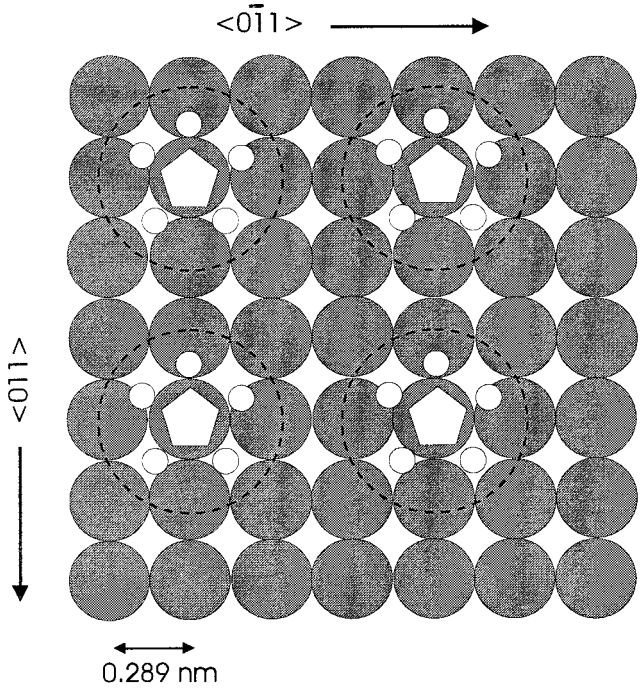


**Figure 4.** Schematic of the ferrocene "footprint" on the Ag(100) substrate. The ferrocene molecule is represented by only one Cp ligand for clarity. The dashed line around the Cp ring system represents the effective van der Waal radius of the Cp ligand idealized into a circle.

through either Ag($\lambda_1$) or the ferrocene overlayer ($\lambda_2$). All numerical values used in eqs 1 and 2 are summarized in Table 2.

Mean free paths of electrons in organometallic solids have not been accurately determined. However, organic materials have been reported[34] with significantly longer mean free paths than metals for comparable electron kinetic energies in this range. Accordingly, lower and upper values for the mean free path of the electron through the ferrocene were estimated by assuming, first, that the mean free path of an electron traveling through ferrocene is not significantly different from that of the silver substrate and, second, that the mean free path of the electron in ferrocene is large enough to be considered infinite. By use of the data in Table 2 and these two approximations, the atomic concentration ratio of carbon to silver on the surface was found to be between 0.7 and 1.5, or approximately 0.07−0.15 ferrocene molecules per surface silver atom. This is a reasonable range for monolayer saturation and corresponds to about one ferrocene interacting with nine silver surface atoms, depicted schematically in Figure 4 with the molecule arbitrarily centered over an atop Ag site.

The 1 ferrocene/9 Ag coverage agrees with previously obtained STM results,[35] although attempts in this study to observe long-range order in the adsorbed ferrocene monolayer

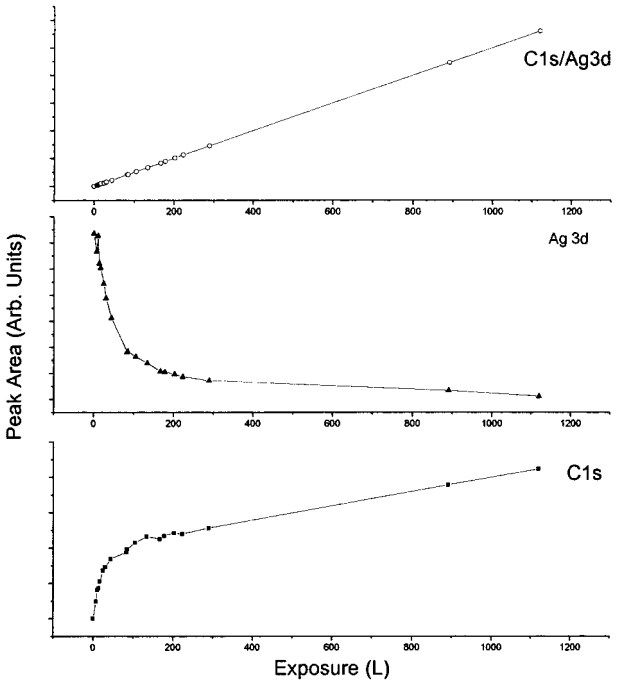


**Figure 5.** Broad range uptake curve of ferrocene. Data were acquired from C 1s and Ag 3d XP spectra at a pass energy of 200 eV. C 1s peak areas are represented by solid squares, Ag 3d peak areas are represented by solid triangles, and peak area ratios are represented by open circles.

with low-energy electron diffraction (LEED) have yet to yield a detectable superstructure. Successive cycles of annealing the ferrocene monolayer at 200 K, just below its desorption temperature, and redosing at 160 K failed either to increase the saturation coverage or to improve the LEED order. Instead, the diffraction features of the (1 × 1) Ag(100) substrate merely broaden and become increasingly diffuse with ferrocene exposure. However, the saturation concentration of ferrocene, which is lower than predicted from simple closest-packing arguments, suggests that some preferred registry of ferrocene exists for the Ag(100) surface, even if this produces only short-range order.

Closest packing of ferrocene molecules, taken as having a circular footprint of approximately 19.7 Å$^2$ based on the size of the Cp ring,[31] yields a concentration of approximately 1 molecule per 4.3 surface Ag. This value is too high for agreement with the XPS monolayer saturation data. Other surface structures for ferrocene that are commensurate with the Ag(100) surface can certainly be envisioned. Attempts to pack the molecules more closely along ⟨011⟩ and ⟨0$\bar{1}$1⟩ in a (2 × 2) structure (0.25 ferrocene/Ag) both bring the Cp rings too close together and produce values of $I_C/I_{Ag}$ that are higher than observed in XPS ($I_C/I_{Ag}$ = 0.038−0.084 calculated from eq 1). A (3$\sqrt{2}$ × 3$\sqrt{2}$)R45°, with 0.22 ferrocenes per surface Ag, is reasonable from the viewpoint of the Cp ring size that includes van der Waal radii but again leads to $I_C/I_{Ag}$ values that are too high (0.035−0.074, eq 1). Whether ferrocene exhibits a long-range commensurate monolayer structure with the Ag(100) or not, it is clear that at saturation coverage the ferrocene monolayer is a fairly open structure.

Figure 5 shows an extended uptake curve taken over a wider range of ferrocene exposures. In this figure, the silver surface was exposed to a successive series of doses ranging from monolayer exposures up to multilayers that should be equivalent to condensed, bulk ferrocene. The peak area ratio, $I_C/I_{Ag}$, is linear with respect to exposure at these longer values, which indicates that the ferrocene films are growing in a layer-by-layer fashion.[36]

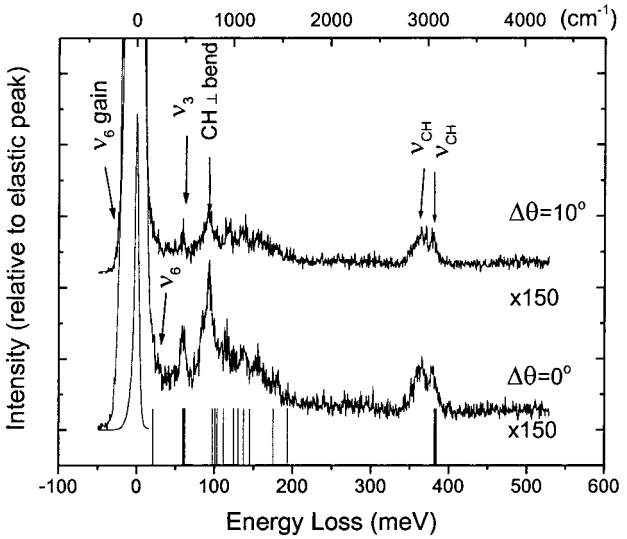


**Figure 6.** HREEL spectra of 9.6 L (~1 monolayer) ferrocene on ($\Delta\theta = 0°$, bottom trace) and off ($\Delta\theta = 10°$, top trace) specular. Solution IR data from ref 19 are added as a series of vertical lines along the *x* axis.

This is supported by observation of a simultaneous exponential decrease in silver 3d intensity with an exponential increase in intensity for the carbon 1s peak.

**B. HREELS Assignments.** The geometry of the ferrocene molecule depends on the temperature and the phase. In the gas phase, the Cp rings in ferrocene are eclipsed and the symmetry[31] of ferrocene is $D_{5h}$. Infrared spectra of crystalline ferrocene[37] at room temperature and 15 K have been obtained for two different types of crystal structures. In both crystalline phases, the symmetry of the individual ferrocene molecules[31] is $D_{5d}$, but at higher temperatures, the molecule gains sufficient energy to overcome the activation barrier of approximately 4−9 kJ/mol [31] for free rotation about the Cp−Fe bonds. All symmetry labels discussed below are assigned relative to the $D_{5d}$ point group unless otherwise noted.

HREEL spectra for approximately one monolayer (9.6 L) of ferrocene in the specular and off-specular directions are presented in Figure 6. A series of vertical lines is displayed along the *x* axis to represent the vibrational modes of the ferrocene molecule observed in solution infrared and Raman spectra.[19] Comparison of the HREEL spectra with the IR/Raman data indicates that except for one loss at 363.3 meV (2930 $cm^{-1}$), a C−H stretching mode that will be discussed below, the vibrational modes observed in HREELS are not significantly perturbed from the solution infrared/Raman energies. This implies that the adsorbate−substrate interaction is fairly weak and that ferrocene is physisorbed on Ag(100) with little rehybridization.

Despite the large number of vibrational modes that overlap in energy, assignments of the losses can be made for the majority of observed loss energies, and these assignments are presented in Table 3. The spectrum is dominated by losses at 59.1 meV (477 $cm^{-1}$) and 92.1 meV (743 $cm^{-1}$), which are the Cp−Fe−Cp $\nu_3$ skeletal mode, depicted in Figure 7, and a perpendicular C−H bending mode, respectively. These modes have previously been identified as characteristic of physisorbed ferrocene.[12,16] The 59.1 meV (477 $cm^{-1}$) $\nu_3$ may overlap with the $\nu_5$ skeletal mode, and evidence for this is provided by the deuterated ferrocene spectrum as discussed below. The two C−H stretching modes present at 363.3 and 378.6 meV (2930 and 3054 $cm^{-1}$) were also previously observed, although they were not resolved from each another.

The modes at 363.3 and 378.6 meV (2930 and 3054 $cm^{-1}$) have been previously assigned[16] to C−H stretching vibrations of $A_{2u}$ and $E_{1u}$ symmetry, respectively. The $\nu_{CH}$ vibrations occur as a single peak in solution[19] but are split into two peaks in HREELS of the adsorbed species. Loss energies and peak structure similar to this have been observed[37] for C−H stretches with $sp^3$ (363.3 meV, 2930 $cm^{-1}$) and $sp^2$ (378.6 meV, 3054 $cm^{-1}$) hybridization. However, these assignments are not consistent with other features of the HREEL spectrum, and it is unlikely that rehybridization explains the appearance of two $\nu_{CH}$ modes. In previous EELS studies of $\eta^5$-$C_5H_5$/Pt(111), Avery[38] also observed two C−H stretching modes at 373.2 and 379.4 meV (3010 and 3060 $cm^{-1}$). These modes were assigned to C−H stretches of $E_2'$ and $E_1' + A_1'$ symmetry, respectively. These assignments are also supported by infrared spectra of crystalline ferrocene[39] where two $\nu_{CH}$ bands are observed at 381.4 and 384.2 meV (3076 and 3099 $cm^{-1}$). Therefore, the loss at 363.3 meV (2930 $cm^{-1}$) is assigned to the $E_{2u}$ stretch and the loss at 378.6 meV (3054 $cm^{-1}$) is assigned to the near-degenerate $E_{1u}$ and $A_{2u}$ C−H stretches shown in Figure 7.

To aid in the remainder of the assignments, HREEL spectra of deuterated ferrocene have been obtained, and these spectra are shown in Figure 8 for monolayer coverage. Deuterated ferrocene shows losses at 57.9, 83.5, and 288.4 meV (467, 673, and 2326 $cm^{-1}$). Comparison with both IR/Raman data for the deuterated analogue[19] and the HREEL spectra shown in Figure 6 indicates that these losses are due to the $\nu_3$ perpendicular C−D bend and the C−D stretching modes, respectively. The energy shifts observed are smaller for skeletal and C−C vibrations than for C−H/C−D vibrations, which is appropriate for the expected isotope effect, in support of the assignments made in Table 3. Additionally, the ferrocene/deuterated ferrocene loss energies observed in the HREEL spectra are in agreement with frequency ratios obtained from infrared/Raman data.[19] At 8.6 meV, the isotope shift for the out-of-plane C−H (C−D) bend is somewhat smaller than anticipated. However, this may be a result of the congestion in the area of the spectrum along with a small protonated ferrocene contaminant in the deuterated spectrum.

The mode at 57.9 meV (467 $cm^{-1}$) in Figure 8 is assigned to the $\nu_3$ mode; deuteration increases the $\nu_3$−$\nu_5$ separation so that the contribution of the $\nu_5$ mode to the loss intensity can now be clearly seen by comparing on- and off-specular HREELS data. In the specular spectrum a combined loss is observed at 57.9 meV (467 $cm^{-1}$), while in the off-specular spectrum the loss now occurs at 63.4 meV (511 $cm^{-1}$) because of the more dramatic decrease in intensity of the dipole-active $\nu_3$ mode. The $\nu_5$ mode, which is not expected to be dipole-active when the molecule adsorbs with its molecular axis perpendicular to the plane of the surface, does not decrease in intensity as rapidly as the detection angle is moved away from the specular geometry. Since the $\nu_5$ loss energy is slightly higher than that of the $\nu_3$ mode, the combined loss intensity shifts to higher energies in off-specular scattering geometries.

The deuterated data are especially important for clarification of the cyclopentadienyl modes between 100 and 200 meV (807 and 1613 $cm^{-1}$) where the spectral congestion in ferrocene is especially dense. For ferrocene, the C−H bending modes occur[19] between 100 and 149 meV (807−1202 $cm^{-1}$). Upon deuteration, these modes are red-shifted[19] by 30 meV (242 $cm^{-1}$) and they are observed in the HREEL spectrum (Figure 8) as a broad band centered at ~90 meV (726 $cm^{-1}$). This band is made up of three perpendicular C−D bending modes at 83.5, 93.9, and 106.7 meV (673, 757, and 860 $cm^{-1}$). Between 130 and 190 meV (1049 and 1532 $cm^{-1}$), we expect[19] to find C−C stretching

**TABLE 3: Assignments for HREEL Spectra Presented in Figures 6 and 8−10**[a]

| mode | | | IR | |
|---|---|---|---|---|
| $Fe(C_5H_5)_2$ | $Fe(C_5D_5)_2$ | assignment | $Fe(C_5H_5)_2$ | $Fe(C_5D_5)_2$ |
| −23.1 (186) | NR | $\nu_6$ ($E_{1u}$) gain | 21.1 (170) | 20.1 (162) |
| 22.6 (182) | 19.5 (157) | $\nu_6$ ($E_{1u}$) | 21.1 (170) | 20.1 (162) |
| 59.1 (477) | 57.9 (467) | $\nu_3$ ($A_{2u}$) | 59.3 (478) | 56.7 (457) |
| NR | 63.4 (511) | $\nu_5$ ($E_{1u}$) | 61.0 (492) | 60.1 (485) |
| | | ⊥ ring distortion ($E_{2u}$) | 62.0 (500) | |
| 92.1 (743) | 83.5 (673) | ⊥ CH bend ($A_{2u}$) | 100.5 (811) | 79.0 (637) |
| 100.6 (811) | 93.9 (757) | ⊥ CH bend ($E_{1u}$) | 103.4 (834) | 84.2 (679) |
| | | $\nu_3 + \nu_1$ ($A_{2u}$) | 97.0 (782) | 92.7 (748) |
| NR | 106.7 (860) | ⊥ CH bend ($E_{2u}$) | 130.2 (1050) | 105.3 (849) |
| 135.9 (1096) | 125.6 (1013) | ring breathing ($A_{2u}$) | 137.4 (1108) | 129.4 (1045) |
| 155.5 (1254) | 137.1 (1106) | $\nu_3$ + ⊥ CH bend ($A_{2u}$) | 159.8 (1289) | 135.7 (1094) |
| 178.6 (1440) | 161.0 (1299) | $\nu_{CC}$ ($E_{1u}$) | 174.9(1411) | 156.2 (1260) |
| 199.3 (1607) | 179.2 (1445) | ⊥ CH bend ($A_{2u}$) double loss | | |
| 363.3 (2930) | 288.4 (2326) | $\nu_{CH}$ ($A_{2u}$) | 382.5 (3085) | 291.9 (2354) |
| | | $\nu_{CH}$ ($E_{1u}$) | 381.3 (3075) | 291.9 (2354) |
| 378.6 (3054) | 288.4 (2326) | $\nu_{CH}$ ($E_{2u}$) | 382.4 (3084) | |

[a] Energies are tabulated in meV with values in wavenumbers in parentheses. Infrared and Raman energies from ref 19. "NR" Stands for "not resolved".

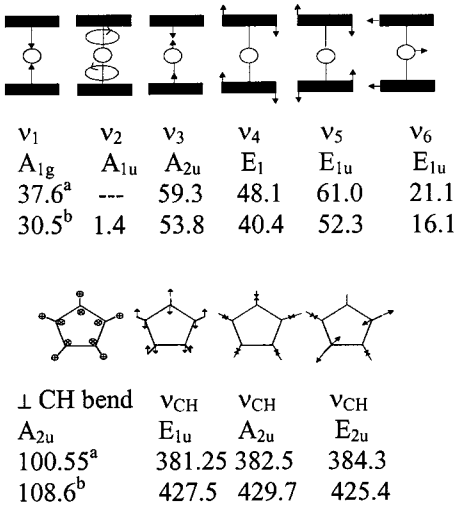


**Figure 7.** Schematic of the vibrational modes of ferrocene used to identify the bonding orientation. Energies reported from refs 19 and 16 (footnotes a and b in the figure) in meV. Arrows indicate motion within the plane of the page and ⊗ or ⊕ symbols indicate motion in or out of the plane of the page.

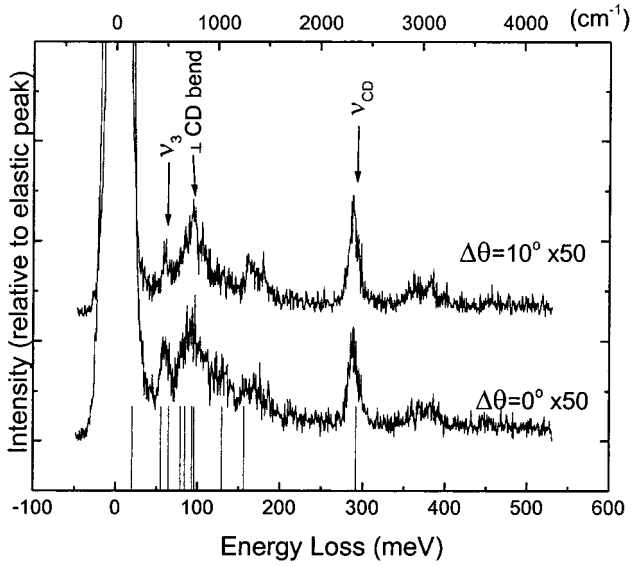


**Figure 8.** HREEL spectra of one monolayer of $Fe(C_5D_5)_2$ with scattering angles as noted in the figure. Solution IR data from ref 19 are added as a series of vertical lines along the *x* axis. The origin of the features observed above 350 meV remains ambiguous. While it is possible that the observed losses are due to combination bands, the possibility of contamination from residual ferrocene cannot be completely ruled out.

vibrations. The modes at 125.6, 137.1, and 161.0 meV (1013, 1106, and 1299 $cm^{-1}$) are assigned to a ring-breathing mode, a combination band, and a C−C vibration, respectively, both by comparison with the ferrocene HREEL spectrum (Figure 6) and by comparison with infrared/Raman data.[19]

HREEL spectra were obtained as a function of exposure over a wide range of surface concentrations and are reported for ferrocene in Figure 9 and deuterated ferrocene in Figure 10. The losses observed in the ferrocene and deuterated ferrocene spectra vary in intensity as exposure is increased but do not vary detectably in energy. The longest exposure shown, at 5825 L, corresponds to condensed, bulk ferrocene, and at this exposure the Ag 3d features in the XP spectrum are almost completely suppressed. For the bulklike ferrocene spectrum, the intensities of the losses observed previously in the low-coverage spectra have decreased significantly with a more rapid drop in signal from losses at higher loss energies than for low-energy losses.

**C. Orientation Effects.** The skeletal modes shown[16,18−19] in Figure 7 are most helpful for elucidating information about the orientation of ferrocene adsorbed on the Ag(100) surface because of the dependence of their intensities with orientation and their relatively high dipole scattering cross sections. In the $D_{5d}$ point group, only modes having $A_{2u}$ or $E_{1u}$ symmetry will be allowed in the HREEL spectrum through dipole-scattering mechanisms. In the present set of data, at low coverages only modes with $A_{2u}$ symmetry are observed to have the proper dipole behavior of being substantially more intense along the specular direction than off-specular. This indicates that the molecule is adsorbed in an upright orientation with the Cp−Fe−Cp molecular axis approximately perpendicular to the plane of the Ag(100) surface. In particular, the $\nu_3$ mode at 59.1 meV (477 $cm^{-1}$) and the perpendicular C−H bend at 92.1 meV (743 $cm^{-1}$) are clearly observed along specular and decrease noticeably in intensity as the detection angle is moved off-specular (Figure 6).

As the exposure is increased beyond monolayer levels, the $\nu_3$ and perpendicular C−H bending modes continuously increase in intensity with no significant change in energy. However, at 71 L, two additional dipole-active modes appear that should only be observed if the molecule tilts or otherwise changes

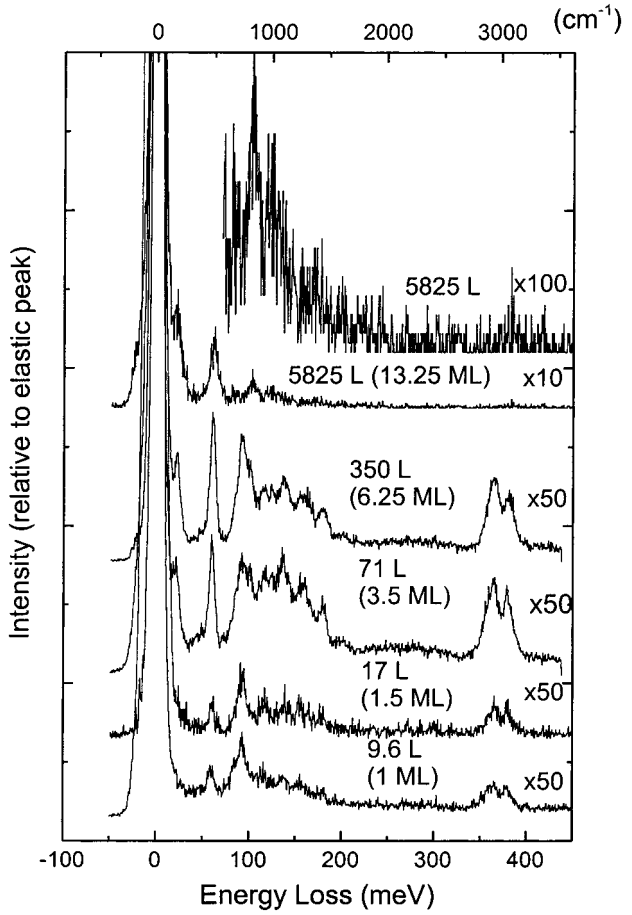


**Figure 9.** HREEL spectra of ferrocene in the specular direction ($\Delta\theta = 0°$) as a function of exposure. Intensities are normalized to the elastic peak intensity.

orientation to allow modes perpendicular to the molecular plane to become dipole-active. These modes are the $\nu_6$ at 22.6 meV (182 $cm^{-1}$) and a perpendicular C−H bend at 100.6 meV (811 $cm^{-1}$). Since both of these modes are of $E_{1u}$ symmetry and are dipole active, the molecular axis must now be canted with respect to the surface normal to allow modes with net dipole moments both parallel and perpendicular to the molecular axis to have significant components along the surface normal. In this orientation, both the $\nu_5$ and the $\nu_6$ (Figure 7) should now be dipole-active as well. While the $\nu_6$ loss is observed in the 5825 L spectrum, the $\nu_5$ loss (solution IR:[19] 61.0 meV, 492 $cm^{-1}$) is not resolved from the $\nu_3$ loss peak.

The intensities of the perpendicular C−H bend, C−H stretches, and modes between 100 and 200 meV (807−1613 $cm^{-1}$) increase up to an exposure of 350 L. At very long exposures, the high energy losses decrease in intensity until at 5825 L the $\nu_6$ and $\nu_3$ modes dominate the observed HREEL spectrum. While these changes are dramatic, they result primarily from the increased contribution from long-range dipole components integrated over the now substantially thick metallocene film. Additionally, the perpendicular C−H bend of $E_{1u}$ symmetry has now become more intense than the lower energy perependicular C−H bend of $A_{2u}$ symmetry at 92.1 meV (743 $cm^{-1}$).

Spectra for deuterated ferrocene (Figure 10) follow the same trends. At low exposures the molecular axis is parallel to the surface normal, and at moderate exposures the molecular axis is canted with respect to the surface normal. As exposure is increased, the skeletal modes ($\nu_3$ and $\nu_6$ at 57.9 and 63.4 meV, respectively) continually increase in intensity. The ring vibrations initially increase in intensity but decrease as the exposures become very long (≥700 L). The $\nu_5$ mode (63.4 meV, 511 $cm^{-1}$) is resolved from the $\nu_3$ (57.9 meV, 467 $cm^{-1}$) in deuterated ferrocene but not in ferrocene. Therefore, in the deuterated ferrocene spectra it is possible to observe the $\nu_5$ mode become dipole-active when the molecular axis becomes canted.

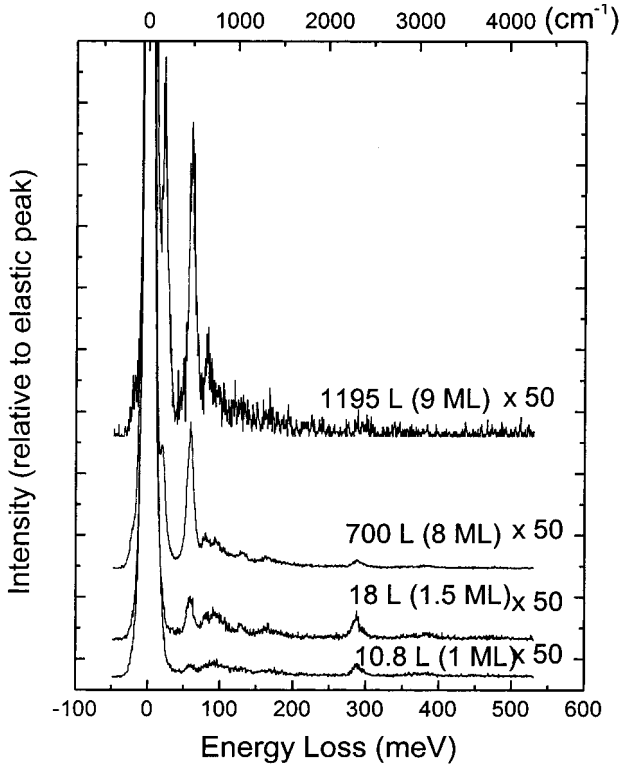


**Figure 10.** HREEL spectra of deuterated ferrocene in the specular direction ($\Delta\theta = 0°$) as a function of exposure. Intensities are normalized to the elastic peak intensity.

The substantial reduction in intensity of the C−H/C−D stretching modes at very long exposures is attributed to the different molecular profile presented by the upright geometry of the monolayer film from the "canted" orientation of the multilayer ferrocene thin film structure. In the monolayer regime, the top Cp ring effectively shadows the underlying molecules and presents primarily C−H stretching loss mechanisms for electron scattering. When the molecular axis tilts relative to the surface normal, the Cp ring no longer is as efficient at shielding the lower part of the molecule and the dipole-active modes become relatively more intense. The canted orientation also apparently presents a much less efficient scattering cross section for the short-range impact scattering mechanism for exciting the C−H stretching modes at these relatively high-loss energies.

**D. HREELS as a Function of Primary Electron Beam Energy.** Comparison of ferrocene HREEL spectra from different sources[12,16,17] often shows similar, but not quite identical, spectra even for surfaces that only weakly physisorb the molecule or for what otherwise should be comparable spectra of condensed, multilayer metallocene. In part this may be due to minor variations in thin film quality or structure, or in slightly different performance of the HREEL spectrometer. However, this may also be due to different choices of primary electron beam energies. Spectra of one monolayer of ferrocene and deuterated ferrocene acquired at a primary beam energy of 1.87 eV are presented in Figure 11. When the data in Figure 11 are compared to data acquired at a beam energy of 3.77 eV (Figures 6 and 8 for ferrocene and deuterated ferrocene, respectively), we immediately note that the dipole-active modes ($\nu_3$ and perpen-

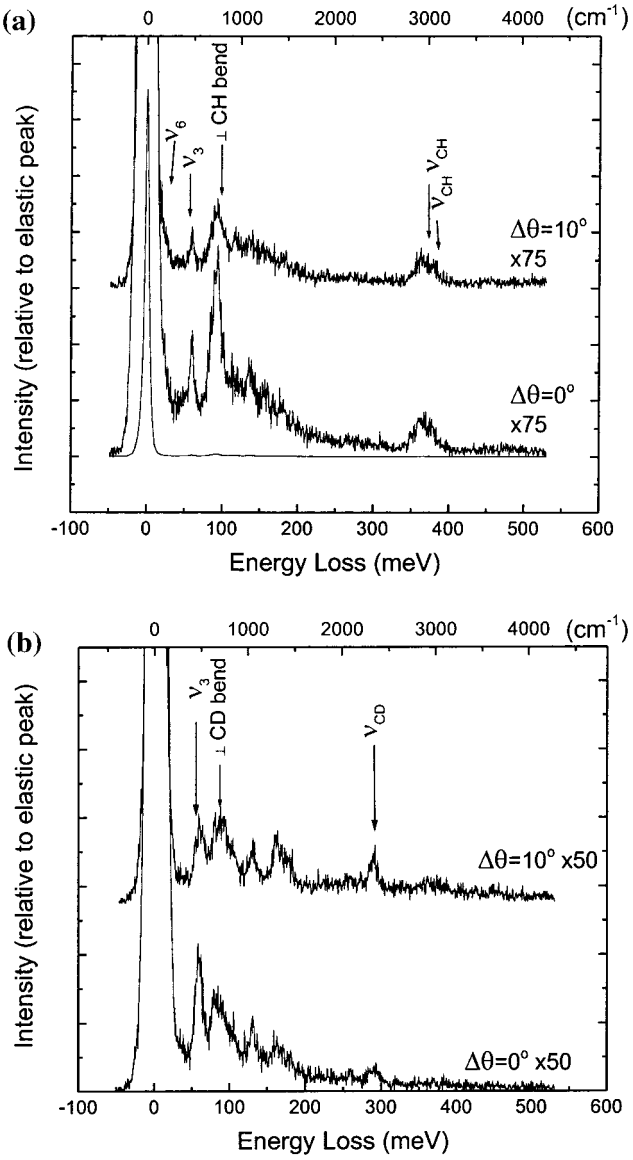


**Figure 11.** HREEL spectra of ~1 monolayer ferrocene (a) and deuterated ferrocene (b) at a primary beam energy of 1.87 eV.

dicular C−H/C−D bend) are much more intense at the lower beam energy.

HREEL spectra of monolayer ferrocene are presented over a wider range in primary beam energies in Figure 12. The data in this figure show that modes with significant dipole character decrease in intensity as the primary beam energy increases in the expected $E^{-1}$ dependence.[40] Since dipole scattering interactions are long-range, the higher kinetic energy electrons have less time to interact with the adsorbate dipole and thus decrease in cross section in direct relationship to the time spent in the near-surface region. Impact-active modes, which result from short-range interactions requiring the electron to penetrate the near-surface region, increase in intensity with primary beam energy over the range studied, in agreement with the $E^1$ dependence of loss intensity expected from electron scattering theory.[40] At a primary beam energy of 1.87 eV, the relative intensities of the four principal modes in Figure 11 are in agreement with previously reported[16] HREEL spectra acquired at a primary beam energy of 1.85 eV.

## IV. Discussion

Both the XP and the HREEL spectra are consistent with ferrocene being physisorbed on the Ag substrate at 150 K.

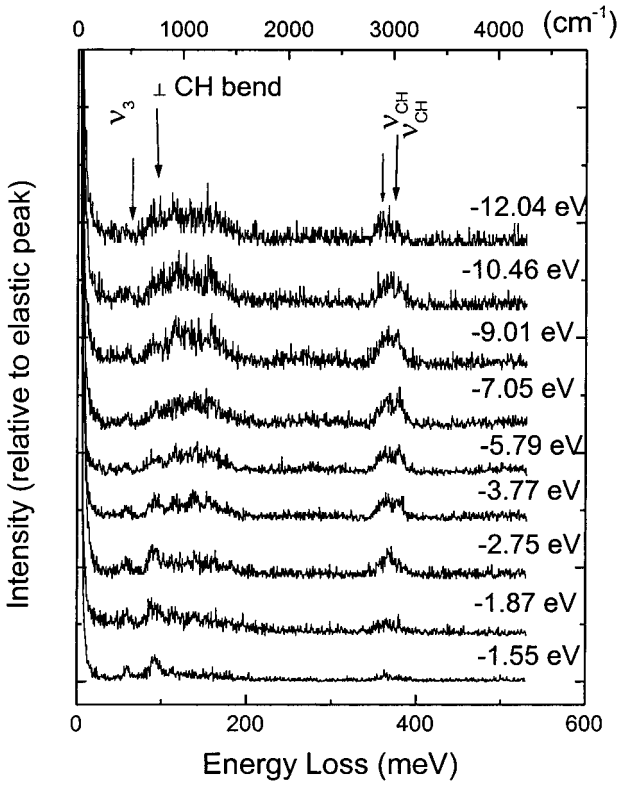


**Figure 12.** HREEL spectra of 11 L ferrocene at $\Delta\theta = 10°$ as a function of primary beam energy. Intensities of individual scans are normalized to their elastic peak intensities.

Spectral data indicate that the interaction between the adsorbed ferrocene and the silver surface is fairly weak as evidenced by the agreement between both binding energies and IR/Raman data reported for bulk ferrocene samples. At low exposures the adsorbed ferrocene molecules possess an upright orientation as evidenced by the strongly dipole-active $\nu_3$ and perpendicular C−H/C−D bend observed in the HREEL spectra. However, upon increasing exposure, the orientation changes from fully upright to one in which the molecular axis is no longer primarily along the surface normal.

There are two possible explanations for the "canted" structure. In bulk ferrocene crystals, adjacent ferrocene molecules have been shown[41] to pack in a herringbone pattern with the hydrogen atoms of one ferrocene's Cp ligands interacting with the iron on the adjacent ferrocene molecule. This not only is a very efficient packing structure but also results in increased van der Waal interactions between the two molecules. Two bulk phases have been observed: an orthorhombic form obtained by crystallization from solution at temperatures below 110 K[42] and a monoclinic form of ferrocene obtained from crystallization at higher temperatures. Once crystallized, the orthorhombic phase can be warmed to temperatures as high as 275 K before conversion to the monoclinic form is observed.[41] As can be seen in Figure 13, both structures would potentially interface well with monolayer ferrocene, which forms with one of its Cp rings approximately parallel to the Ag(100) surface. Either form would also have a significant component of its molecular axis tilted away from the substrate surface normal.

At the very longest exposures, the C−H/C−D modes observed in the HREEL spectra are weak compared to other vibrational modes and the $\nu_6$, $\nu_3$, and perpendicular CH bend losses dominate the spectrum. This reduction in intensity is attributed to the decrease in cross section for impact scattering mechanisms for C−H vibrational stretching modes in the Cp

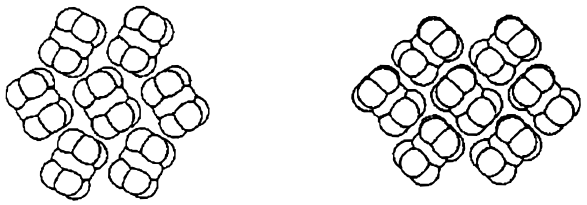


**Figure 13.** Schematic depiction of the orthorhombic and monoclinic crystalline forms of bulk ferrocene.

ring. A related molecule, nickelocene, shows similar HREELS behavior as a function of metallocene coverage.[43] As the exposure is increased, its orientation undergoes a change from upright, with dipole-active modes only observed if they have a significant component along the molecular axis, to apparently "canted" with both parallel and perpendicular vibrational symmetry, giving rise to dipole losses. At very long exposures leading to multilayer concentrations the intensity of the C−H stretching modes in nickelocene is also reduced.

Unfortunately, with our techniques we were not able to rule out a second possibility that the multilayer coverages of ferrocene adsorb in a disordered manner and that the "canted" molecular axis represents an average over a number of molecular orientations as the film randomizes. Unless the film is truly amorphous, the degree of disorder in the film might be expected to be improved by annealing, slower deposition, or adsorption at slightly different substrate temperatures. We have not been able to obtain well-ordered LEED patterns on either monolayer or multilayer ferrocene films, but the quality of the diffraction pattern from the underlying Ag(100) lattice has been observed to degrade in quality as the ferrocene adsorbate layer thickens. Additionally, the HREEL spectral quality also appears to degrade for the longest of exposures. It is tempting to cite these results as indication of poor film order. However, even well-ordered Langmuir−Blodgett and self-assembling organic films show only poor electron scattering characteristics in LEED and HREELS. The degree to which disorder contributes to the present observations therefore cannot easily be quantified.

## V. Conclusions

XPS has been used to characterize the chemical state of ferrocene as well as the manner in which films of ferrocene grow. We find that the C 1s binding energy is consistent with carbon in an aromatic ring and that the Fe $2p_{3/2}$ binding energy is consistent with positively charged iron. The carbon uptake is linear over all exposures, which indicates that the ferrocene films are growing in a layer-by-layer fashion.

HREEL spectra of ferrocene and deuterated ferrocene indicate that ferrocene is adsorbed molecularly with its molecular axis parallel to the surface normal. The nominal energy shift of modes observed in the HREEL spectra indicates that ferrocene is physisorbed on the Ag(100) substrate. The orientation is maintained up to moderate multilayer exposures, but the molecular axis becomes canted with respect to the surface normal for multilayer thin films.

**Acknowledgment.** The authors are grateful for support from AFOSR under Grant F46920-94-1-0018, from the ACS Petroleum Research Foundation under Grant 31708-AC, and from the University of Nebraska Center for Materials Research and Analysis. We also thank P. A. Dowben for his numerous helpful discussions.

## References and Notes

(1) Kealy, T. J.; Pauson, P. L. *Nature* **1951**, *168*, 1039. Miller, S. A.; Tebboth, J. A.; Tremaine, J. F. *J. Chem. Soc.* **1951**, 632.

(2) Johnson, J. L. *Metallocene Technology*; Noyes Data Corporation: NJ, 1973.

(3) Lewis, R. J., Sr. *Hawley's Condensed Chemical Dictionary*, 12th ed.; Van Nostrand-Reinhold Co.: New York, 1993.

(4) Okawa, Y.; Nagano, M.; Watanabe, M. *Biosens. Bioelectron.* **1999**, *14*, 229.

(5) Ion, A.; Ion, I.; Saint-Aman, E. *Adv. Mater.* **1997**, *9*, 711.

(6) Tajima, K.; Huxur, T.; Koshinuma, M. *Colloids Surf. A* **1995**, *94*, 243.

(7) Ying, Z. C.; Ho, W. *J. Chem. Phys.* **1990**, *93*, 9077 and references therein.

(8) Cook, J. C.; McCash, E. M. *Surf. Sci.* **1996**, *364*, L605.

(9) Greenwood, N. N.; Earnshaw, A. *Chemistry of the Elements*; Pergamon Press: New York, 1984.

(10) Dyagileva, L. M. *Russ. J. Phys. Chem.* **1996**, *67*, 1071.

(11) Welipitiya, D.; Green, A.; Woods, J. P.; Dowben, P. A.; Robertson, B.; Byun, D.; Zhang, J. *J. Appl. Phys.* **1996**, *79*, 8730.

(12) Welipitiya, D.; Dowben, P. A.; Zhang, J.; Pai, W. W.; Wendelken, J. F. *Surf. Sci.* **1996**, *367*, 20.

(13) Pai, W. W.; Zhang, J.; Wendelken, J. F.; Warmack, R. J. *J. Vac. Sci. Technol. A* **1997**, *15*, 785.

(14) Welipitiya, D.; Borca, C. N.; Waldfried, C.; Hutchings, C.; Sage, L.; Woodbridge, C. M.; Dowben, P. A. *Surf. Sci.* **1997**, *393*, 63.

(15) Thibaudau, F.; Roche, J. R.; Salvan, F. *Appl. Phys. Lett.* **1994**, *64*, 523.

(16) Waldfried, C.; Welipitiya, D.; Hutchings, C. W.; de Silva, H. S. V.; Gallup, G. A.; Dowben, P. A.; Pai, W. W.; Zhang, J.; Wendelken, J. F.; Boag, N. M. *J. Phys. Chem. B* **1997**, *101*, 9782.

(17) Durston, P. J.; Palmer, R. E. *Surf. Sci.* **1998**, *400*, 277.

(18) Nakamoto, K. *Infrared and Raman Spectra of Inorganic and Coordination Compounds*, 4th ed.; John Wiley and Sons: New York, 1986; p 391.

(19) Lippincott, E. R.; Nelson, R. D. *Spectrochim. Acta* **1958**, *10*, 307.

(20) Brunvoll, J.; Cyvin, S. J.; Schäfer, L. *J. Organomet. Chem.* **1971**, *27*, 107.

(21) Pugmire, D. L.; Woodbridge, C. M.; Root, S.; Langell, M. A. *J. Vac. Sci. Technol. A* **1999**, *17*, 1581.

(22) Muilenberg, G. E. *Handbook of X-Ray Photoelectron Spectroscopy*; Perkin-Elmer Corporation: Minnesota, 1979.

(23) Berrie, C. L.; Langell, M. A. *Surf. Interface Anal.* **1991**, *17*, 635. Berrie, C. L.; Langell, M. A. *Surf. Interface Anal.* **1994**, *21*.

(24) Briggs, D.; Seah, M. P. *Practical Surface Analysis*, 2nd ed.; John Wiley and Sons: New York, 1990; Vol. 1, Chapter 3.

(25) Barber, M.; Connor, J. A.; Derrick, L. M. R.; Hall, M. B.; Hillier, I. H. *J. Chem. Soc., Faraday Trans. 2* **1973**, *69*, 559.

(26) Gassman, P. G.; Macomber, D. W.; Hershberger, J. W. *Organometallics* **1983**, *2*, 1470.

(27) Cook, D. B. *Int. J. Quantum Chem.* **1992**, *43*, 197.

(28) Scofield, J. H. *J. Electron Spectrosc. Relat. Phenom.* **1976**, *8*, 129.

(29) Ref 25, Chapter 5.

(30) Penn, D. R. *J. Electron Spectrosc. Relat. Phenom.* **1976**, *9*, 29.

(31) Takasugawa, F.; Koetzle, T. F. *Acta Crystallogr. B* **1979**, *35*, 1074. Seiler, P.; Dunitz, J. D. *Acta Crystallogr. B* **1979**, *35*, 1068.

(32) Cotton, F. A.; Wilkinson, G. *Advanced Inorganic Chemistry*, 3rd ed.; John Wiley & Sons: New York, 1972; p 120.

(33) Langell, M. A.; Berrie, C. L.; Nassir, M. H.; Wulser, K. W. *Surf. Sci.* **1994**, *320*, 250.

(34) Gries, W. H. *Surf. Interface Anal.* **1996**, *24*, 35 and references therein.

(35) Dowben, P. A. Unpublished results.

(36) Vook, R. W. *Int. Met. Rev.* **1982**, *27*, 209.

(37) Biener, J.; Schenk, A.; Winter, B.; Lutterloh, C.; Schubert, U. A.; Küppers, J. *Surf. Sci.* **1993**, *291*, L725.

(38) Avery, N. R. *Surf. Sci.* **1984**, *137*, L109.

(39) Rocquet, F.; Berreby, L.; Marsault, J. P. *Spectrochim. Acta A* **1978**, *29*, 1101.

(40) Ibach, H.; Mills, D. L. *Electron Energy Loss Spectroscopy and Surface Vibrations*; Academic Press: New York, 1982; Chapter 3.

(41) Braga, D.; Grepioni, F. *Organometallics* **1992**, *11*, 711.

(42) Seiler, P.; Dunitz, J. D. *Acta Crystallogr. B* **1982**, *38*, 1741.

(43) Pugmire, D. L.; Woodbridge, C. M.; Langell, M. A. *Surf. Sci.* **1998**, *411*, L844.